Modified drought severity index: model improvement and its application in drought monitoring in China

Peng Sun[1a], Zice Ma[1a], Qiang Zhang[2,3*], Vijay P. Singh[4], Chong-Yu Xu[5]

1. School of Geography and Tourism, Anhui Normal University, Anhui 241002, China.
2. State Key Laboratory of Earth Surface Processes and Resource Ecology, Beijing Normal University, Beijing 100875, China;
3. Faculty of Geographical Science, Beijing Normal University, Beijing 100875, China;
4. Department of Biological and Agricultural Engineering and Zachry Department of Civil & Environmental Engineering, Texas A&M University, College Station, Texas, USA; National Water and Energy Center, UAE University, Al Ain, UAE;
5. Department of Geosciences and Hydrology, University of Oslo, P O Box 1047 Blindern, N-0.16 Oslo, Norway.

Corresponding author: zhangq68@bnu.edu.cn

[a] Peng Sun and Zice Ma contributed equally to this work.

Abstract: With advancement of remote sensing techniques, remote-sensing drought indices have been widely used for drought monitoring. However, the monitoring accuracy of a specific drought index regionally varies. Considering the deficiency of existing drought indices in reflecting vegetation growth, here we propose a Modified Drought Severity Index (MDSI) with local optimization method constrained by the inclusion of vegetation greenness, crop water shortage, canopy temperature, vegetation structure, and physiological status. We evaluated drought monitoring performance of MDSI across China, and detected high correlations between MDSI and soil moisture (SM), Standardized Precipitation Index at a 3-month scale (SPI-3), actual drought-affected areas (ADA), evidencing higher drought performance of MDSI when compared to 8 widely-used drought indices. Besides, MDSI performed better in monitoring agricultural drought. We found amplifying short-term drought intensity in the future. Ecological restoration and cultivated land reclamation can alleviate drought effects. However, urbanization can potentially intensify droughts. How to adapt human behavior to droughts is a challenging task.

Key words: Modified Drought Severity Index; Drought monitoring; Soil moisture; Drought-affected croplands; Spatiotemporal pattern

1. Introduction

The United Nations proposed sustainable development goals (SDGs) in 2015 which include 17 goals and 169 targets. Droughts directly exacerbates water stress and hence threatens food security, and causes ecological crisis and poverty and hampers sustainable development (Pradhan et al., 2017; Zhang and Yuan, 2020). Drought is usually viewed as one of the costliest natural hazards over the globe (Mishra and Singh, 2010; Zargar et al., 2011; Zhang et al., 2015; Shen et al., 2022), causing damaging impacts on society and eco-environment (Zhang et al., 2017). Global economic losses caused by droughts have been estimated to be as high as 6 to 8 billion US dollars annually, far larger than those caused by other meteorological disasters (Wilhite, 2000). Furthermore, accelerated hydrological cycle can be expected in the backdrop of global warming (Allen and Ingram, 2002; Zhang et al., 2013), which potentially increases the frequency and/or intensity of climate extremes at regional and global scales, such as floods and droughts (Li et al., 2015; Hu et al., 2018). Therefore, to achieve sustainable development in China renders it necessary to develop scientific mitigation strategies for drought risks (Battisti and Naylor, 2009; He et al., 2017; Zhang et al., 2019).

Drought indices have been widely used in the analysis and monitoring of drought events (Um et al., 2018). The first step for drought analysis is to develop an appropriate drought monitoring index (Coats & Mankin, 2016; Zhang et al., 2018). Due to the complexity of droughts, there are multiple drought indices (e.g. Sun et al., 2017). Compared to meteorological drought index, remote sensing monitoring provides continuous spatiotemporal monitoring of dynamic change of the earth's surface (Ma et al., 2021), including nonparametric integrated agrometeorological drought monitoring (Zhang et al., 2018), Vegetation Condition Index (VCI) (Kogan, 1995), Vegetation Supply Water Index (VSWI) (Carlson et al., 1994), Temperature Condition Index (TCI) (Kogan, 1995), Crop Water Stress Index (CWSI) (Jackson et al., 1981, 1988), and Temperature Vegetation Dryness Index (TVDI) (Sandholt et al., 2002). Mu et al. (2013) integrated MODIS data, actual evapotranspiration, potential evapotranspiration (PET), and Normalized Difference Vegetation Index (NDVI) data in studying effects of droughts on soil moisture. However, the influencing factors considered in the development of these drought indices are assumed to be spatially homogeneous and cannot reflect spatial complexity of drought conditions.

Mu et al. (2013) proposed a Drought Severity Index (DSI) based on moderate resolution imaging spectroradiometer (MODIS)-based evapotranspiration (ET), potential evapotranspiration (PET), and Normalized Difference Vegetation Index (NDVI). DSI has been widely used in drought monitoring (e.g. Um et al., 2018). However, NDVI cannot well reflect the growth status of vegetation and has a certain lag (Agutu et al., 2017). Kogan et al. (2012) proposed the Vegetation Health Index (VHI), based on the impact of moisture and heat on vegetation, describing greenness, vitality, and thermal status of vegetation canopy (Kogan et al., 2012; Bokusheva et al., 2016; Li et al., 2020). Leaf Area Index (LAI) can well reflect vegetation structure and physiological parameters, and some previous studies found decreased LAI due to water shortage (Fisher et al., 2007; Yazdani et al., 2007). Mu et al. (2018) compared DSI (Drought Severity Index) and PDSI (Palmer Drought Severity Index) during the growing season and evaluated the applicability of DSI in drought monitoring, but did not evaluate DSI from multiple time scale perspectives. From the perspective of vegetation growth, it is critical to consider responses of vegetation canopy temperature, vegetation structure and physiological parameters to regional agricultural drought. In addition, DSI is the sum of crop water stress index (ET/PET) and vegetation greenness index (NDVI) on the basis of equal weight. However, obvious spatial heterogeneity in climate changes may differentiate combination values of different regional weights.

Hence, calculation of DSI should include multiple vegetation-related limiting factors and weights of each vegetation-related limiting factors in different regions. To address these issues, the objective of this study is to develop and evaluate a Modified Drought Severity Index (MDSI) based on remote sensing data for agricultural drought monitoring under different underlying surface conditions. The constrained optimization method was adopted to decide the local optimal weights for MDSI across China (Powell., 1978; Hao et al., 2015). Our approach uses local optimal weights to integrate single agricultural drought-related variables. Local optimal weights were selected to use regionally-varying weights to reflect spatial heterogeneity of droughts. The MDSI was integrated with agricultural drought-related variables, such as vegetation greenness, water stress of crops, vegetation canopy temperature, vegetation structure and physiology, derived from MODIS and GLASS. Considering that Standardized Precipitation Evapotranspiration Index (SPEI) has the advantage over Standardized Precipitation Index (SPI) in the mathematical calculation of water balance and over PDSI in multi scalar analysis, SPEI at 3-month scale (SPEI-3) can reveal regional agricultural drought to a certain extent, and SPEI has been widely applied in drought monitoring across China (Vicente-Serrano et al., 2010; Seibert et al., 2012; Beguería et al., 2014; Yu et al., 2014; Xu et al., 2015; Ye et al., 2019). Thus, this study used SPEI-3 as the in-situ index and agricultural drought-related variables to determine the local optimal weight of each variable and calculate MDSI by a constrained optimization method.

The objectives of this study therefore were to (1) develop MDSI for monitoring agricultural drought in China; (2) compare AVI (Anomaly Vegetation Index) (Huete, 1988; Sun et al., 2017), VCI, VSWI, TCI, CWSI, TVDI, DSI, VHI (denoted simply as DI hereafter), and MDSI to evaluate the applicability of MDSI in drought monitoring across China based on soil moisture, precipitation, and actual drought-affected area; (3) monitor agricultural drought using MDSI at different time scales across China; and (4) quantify the impacts of underlying surface changes on drought tendencies using land use conversion datasets.

2. Data

Here we analyzed daily precipitation, minimum temperature, maximum temperature, relative humidity, sunshine hours and wind speed data sourced from the National Meteorological Information Center of the China Meteorological Administration (http://data.cma.cn/). To ensure the integrity and continuity of the data series, stations with missing data of >1% were removed from analysis. We selected 1957 meteorological stations (Fig. 1d) spanning 1980–2019 across China for ongoing analysis. The Moderate Resolution Imaging Spectroradiometer (MODIS) composite 8-day ET and PET with 0.5 km resolution, monthly LST with ×0.05° resolution, and monthly NDVI with 1 km resolution for the period of 2001–2018 were obtained from National Aeronautics and Space Administration’s (NASA, https://modis.gsfc.nasa.gov/). The GLASS 8-day LAI data from 2001 to 2018 were obtained from http://glass-product.bnu.edu.cn/ (Li et al., 2018).

The monthly SM data with 0.5°×0.5° spatial resolution for the period of 2001–2018 was used in this study and the dataset was sourced from the U.S. Climate Prediction Center (https://www.esrl.noaa.gov/). The data were tested and validated with in situ SM. In spite of its simplicity, the product matched the seasonal and interannual variability of in situ SM fairly well (Dirmeyer et al, 2004; Wu et al., 2015). The data were calculated on a daily time step based on the water balance in the soil by a layered hydrological model (Fan et al., 2004).

The vegetation type data were sourced from the Resource and Environment Data Center of the Chinese Academy of Sciences at http://www.resdc.cn/ (Fig. 1a). The remotely sensed Land use/land cover change (LUCC) data with a 1 km resolution across China from 2000 to 2018 were sourced from the Resource and Environment Data Center, Chinese Academy of Sciences (http://www.resdc.cn/). We calculated and mapped the spatial distribution of the converted land use pattern from 2000 to 2018, and subdivided the land use pattern into unchanged areas, reclaimed land cover (land types reclaimed for woodland and grassland, or from grassland to woodland); urban expansion areas, i.e. built-up land; cultivated land reclamation areas (land conversion from other land covers into cropland); and grassland degradation areas (degraded grassland) (Fig. 1b). The actual irrigation areas were sourced from the Irrigated Area Map Asia and Africa prepared by International Water Management Institute (Fig. 1c) (Zhang et al., 2018). The actual drought-affected areas (ADA) of each province in China during 2001 to 2018 were sourced from the National Bureau of Statistics (https://data.stats.gov.cn/).

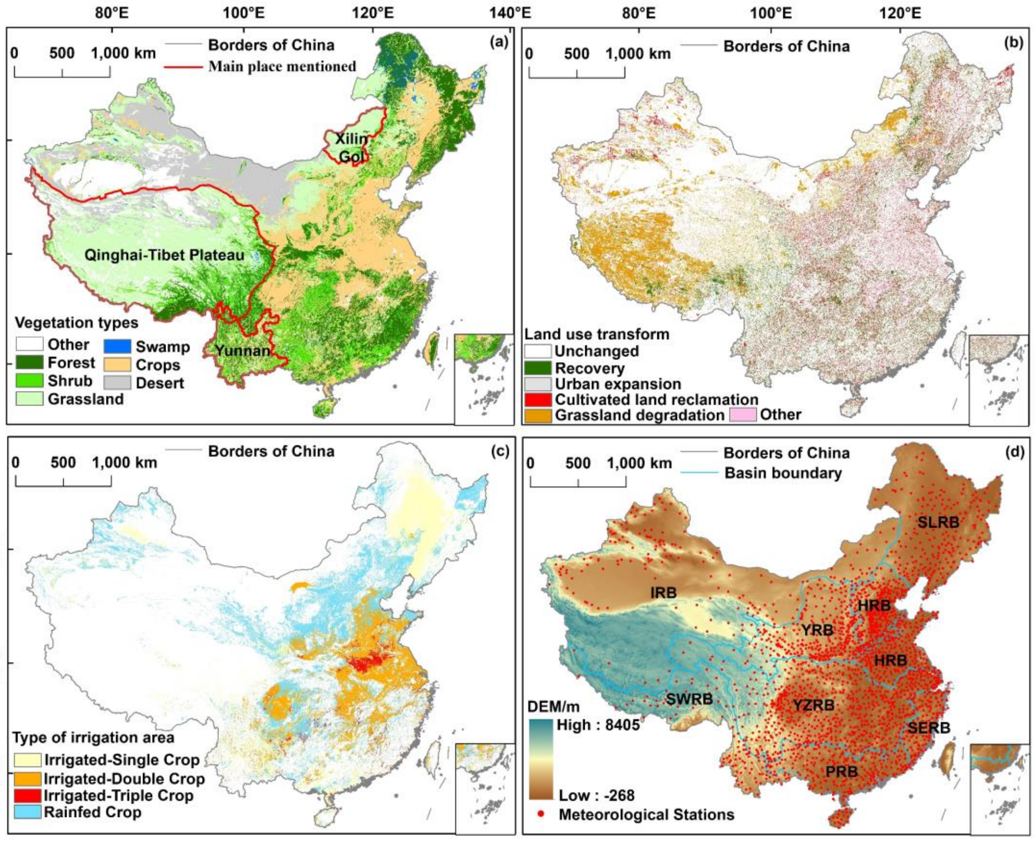

Fig. 1 Spatial pattern of vegetation types (a), land use transform (b), actual irrigation area (c) and altitude and locations of the 9 major river basins and meteorological Station (d) by Resource and Environment Science and Data Center across China. These 9 major river basins include Songliao River Basin (SLRB), Hai River Basin (HARB), Huai River Basin (HURB), Yellow River Basin (YRB), Yangtze River Basin (YZRB), Pearl River Basin (PRB), Southeast River Basin (SERB), Southwest River Basin (SWRB) and Inland River Basin (IRB).

3. Methods

The framework shown in Fig. 2 describes overall processes of developing an agricultural drought monitoring model and analyzing its applicability based on MODIS data and GLASS LAI data in this study.

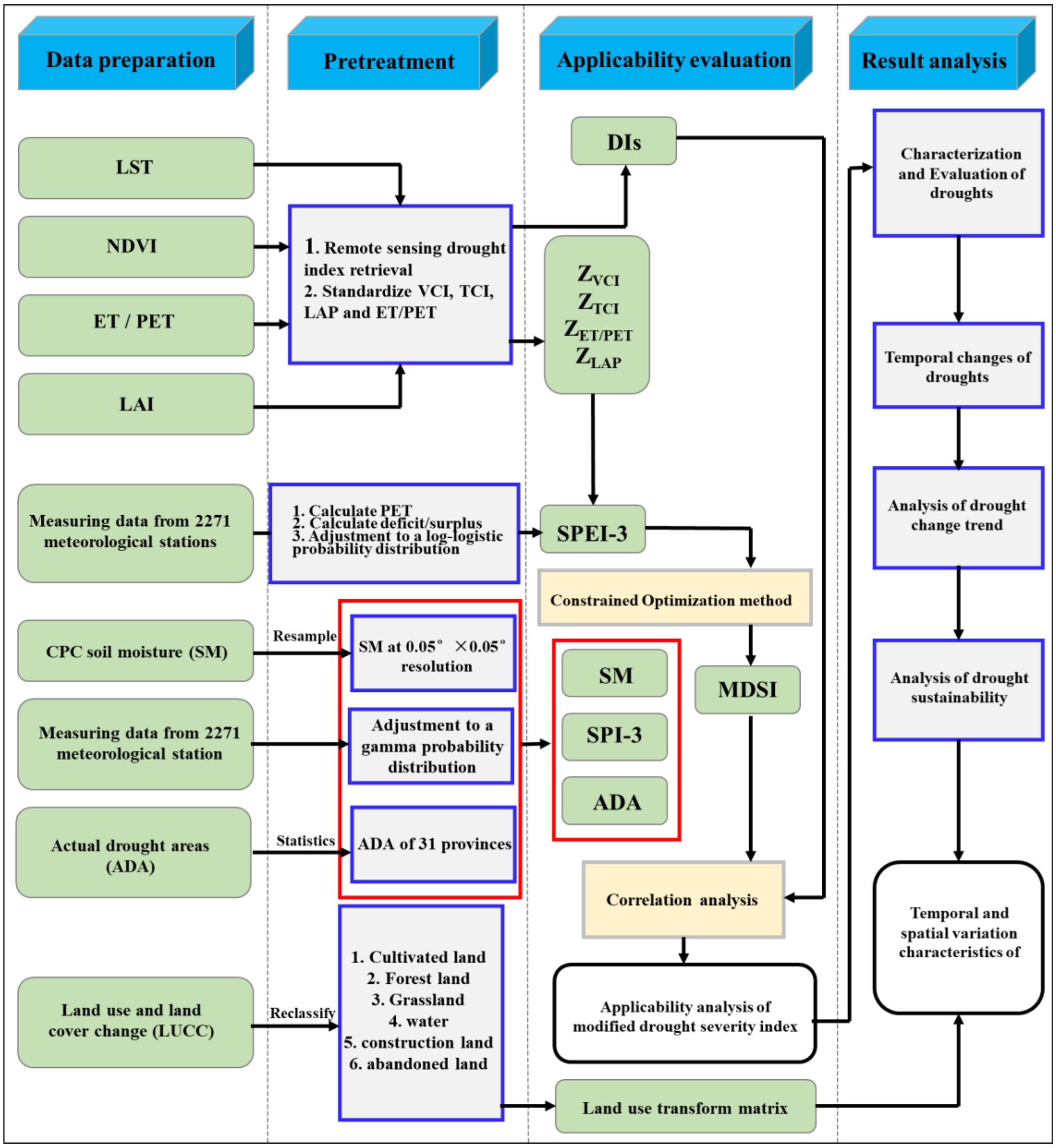

Fig. 2 A analysis framework for building a modified drought severity Index model.

3.1 Meteorological drought index

The SPI and SPEI were introduced by Mckee et al. (1993) and Vicente-Serrano et al. (2010), respectively. The 1-month SPI/SPEI has been used to monitor meteorological drought. 3-month SPI/SPEI can reflect soil moisture changes and the 12-month SPI/SPEI the long-term changes in run off, groundwater, and freshwater storage (Mishra and Singh, 2010). Therefore, we applied SPEI-3 as the in-situ index and the variables related to crop growth were used to calculate MDSI by a constrained optimization method. SPI-3 was used to verify the sensitivity of MDSI to precipitation

3.2 Modified Drought Severity Index (MDSI)

There are 8 widely-used DIs, i.e. AVI, VCI, VSWI, TCI, CWSI, TVDI, DSI and VHI, which can be categorized into three groups: (1) drought indices considering vegetation growth, such as AVI, VCI, VSWI, TCI, TVDI, and VHI; (2) drought index considering crop water stress only such as CWSI; and (3) drought indices considering vegetation growth and SM such as DSI. DSI combines NDVI, ET and PET, where NDVI describes vegetation growth changes, the ratio of ET to PET better reflects the energy and water exchange among vegetation, soil and atmosphere, and can describe crop water stress (Allen et al., 2011; Cooke et al., 2012; Park et al., 2016; Huang et al., 2018). More detailed descriptions can be found in Table 1 (Jackson et al., 1981, 1988; Chen et al., 1994; Carlson et al., 1994; Kogan, 1995; Sandholt et al., 2002; Kogan, F., 2012; Mu et al., 2013).

Table 1 Remote sensing-based drought indices considered in this study

Indices	Variables	Equations
AVI	NDVI	$AVI = NDVI_i - \overline{NDVI}$
VCI	NDVI	$VCI = \frac{NDVI_i - NDVI_{min}}{NDVI_{max} - NDVI_{min}}$
VSWI	NDVI, LST	$VSWI = \frac{NDVI_i}{LST_i}$
TCI	LST	$TCI = \frac{LST_{max} - LST_i}{LST_{max} - LST_{min}}$
CWSI	ET, PET	$CWSI = 1 - \frac{ET}{PET}$
TVDI	NDVI, LST	$LST_{NDVI,min} = a_1 + b_1 \times NDVI$ $LST_{NDVI,max} = a_2 + b_2 \times NDVI$ $TVDI = \frac{(LST - LST_{NDVI,min})}{(LST_{NDVI,max} - LST_{NDVI,min})}$

DSI	ET, PET, NDVI	$Z_{NDVI} = \frac{NDVI - \overline{NDVI}}{\sigma_{NDVI}}$ $Z_{\frac{ET}{PET}} = \frac{\frac{ET}{PET} - \overline{\frac{ET}{PET}}}{\sigma_{\frac{ET}{PET}}}$ $Z_1 = Z_{NDVI} + Z_{\frac{ET}{PET}}$ $DSI = \frac{z_1 - \overline{z_1}}{\sigma_1}$
VHI	NDVI, LST	VHI=0.5×VCI+0.5×TCI

The algorithm of MDSI is as follows. The first step is to calculate the index reflecting the greenness (VCI), temperature (TCI), vegetation structure, and physiological parameters (LAP) of the vegetation canopy:

$$VCI = \frac{NDVI_i - NDVI_{min}}{NDVI_{max} - NDVI_{min}} \quad (1)$$

$$TCI = \frac{LST_{max} - LST_i}{LST_{max} - LST_{min}} \quad (2)$$

$$LAP = \frac{LAI_i - \overline{LAI}}{\overline{LAI}} \quad (3)$$

While NDVI is the normalized difference vegetation index, LST is the surface temperature, LAI is the leaf area index, $*_i$ is the * value of the variable during the *i*th period within a certain year, *max is the maximum value of the variable in the *i*th period within a certain year, *min is the minimum value of the variable in the *i*th period within a certain year, $\overline{*}$ is the multi-year average value of the *variable during the *i*th period within a certain year.

The second step is to standardize VCI, TCI, LAP and ET/PET:

$$Z_{Index} = \frac{Index_i - \overline{Index}}{\sigma_{Index}} \quad (4)$$

where $Index_i$ is the value of the variable during the *i*th period of within a certain year, σ_{Index} is the standard deviation of Index, and $\overline{Index}$ is the multi-year average of the index variable during the *i*th period within a certain year. Z_{Index} is VCI, TCI, LAP and $\frac{ET}{PET}$ standardized by the Z-score. Z_{VCI} denotes the greenness of the vegetation canopy. The larger the Z_{VCI} value, the better the vegetation growth condition. Z_{TCI} describes the temperature of the vegetation canopy. The larger the Z_{TCI} value, the weaker the effect of temperature stress on vegetation growth. Z_{LAP} indicates the structure and physiological parameters of vegetation. The larger the Z_{LAP} value, the stronger the photosynthesis of vegetation. $Z_{\frac{ET}{PET}}$ expresses crop water stress information such that the larger the $Z_{\frac{ET}{PET}}$ value the weaker the vegetation under water stress.

Taking SPEI-3 as the in-situ index, we summed up Z_{VCI}, Z_{TCI}, Z_{LAP} and $Z_{\frac{ET}{PET}}$, based on the optimal weight from the constrained optimization method, and then we obtained the MDSI as:

$$f(X,Y) = max\left(\frac{E[(X-\mu X)\times(Y-\mu Y)]}{\sigma X \times \sigma Y}\right) \tag{5}$$

$$\text{X = SPEI-3} \tag{6}$$

$$O = \alpha \times Z_{VCI} + \beta \times Z_{TCI} + \gamma \times Z_{LAP} + (1-\alpha-\beta-\gamma) \times Z_{\frac{ET}{PET}} \tag{7}$$

$$\begin{cases} 0 < \alpha < 1 \\ 0 < \beta < 1 \\ 0 < \gamma < 1 \end{cases} \tag{8}$$

$$MDSI = \frac{O_i - \bar{O}}{\sigma_O} \tag{9}$$

While $f(X,Y)$ is the highest correlation between *X* and *Y*; *Y* is the comprehensive standard score derived from Z_{VCI}, Z_{TCI}, Z_{LAP} and $Z_{\frac{ET}{PET}}$; *X* is the in situ index SPEI-3; σ_Y is the standard deviation of Y; Y_i is value of the variable during the *i*th period within a certain year; $\bar{Y}$ is the multi-year average value of the *Y* variable during the *i*th period within a certain year. MDSI is a modified version of DSI. Positive MDSI shows wet conditions and higher MDSI shows wetter conditions and vice versa.

However, one issue about the constrained optimization method is regionally varying weights, irrespective of regional differences across the underlying surface. Therefore, based on the pixel scale and in-situ drought index, this study calculated the optimal weights of different agricultural drought-related variables to improve the regional applicability of constrained optimization method. Both MDSI and DSI are defined by the Z-score. The MDSI proposed in this study follows the Normal distribution (average value is 0, standard deviation is 1). Since they have the same drought and humidity monitoring results, the same drought and humidity classification standards can be used (Zhang and Yamaguchi, 2014) (Table 2).

Table 2 Categories and wetness/dryness conditions related to different MDSI values

Categories	Wet/dry intensities	MDSI values
W_5	Extremely wet	≥1.50
W_4	Very wet	1.20≤MDSI<1.50
W_3	Moderate wet	0.90≤MDSI<1.20
W_2	Slight wet	0.60≤MDSI<0.90
W_1	Incipient wet	0.30≤MDSI<0.60
WD	Normal	-0.30≤MDSI<0.30
D_1	Incipient dry	-0.60≤MDSI<-0.30
D_2	Slight dry	-0.90≤MDSI<-0.60
D_3	Moderate dry	-1.20≤MDSI<-0.90
D_4	Heavy dry	-1.50≤MDSI<-1.20
D_5	Extremely dry	<-1.50

3.3 T-test of the correlation coefficient

The correlation coefficient is a statistical indicator showing the degree of correlation between two variables. In this study, we used the correlation coefficient to quantify the correlation between DIs and SM, and between SPI-3 and ADA at the pixel scale. The significance of the correlation coefficient was evaluated using the T-test.

3.4 Sen's slope and modified Mann-Kendall trend test

Sen's slope is a robust non-parametric statistical method for the detection of trends and is widely used for meteorological, hydrological, and vegetation data (Theil, 1992). The modified Mann-Kendall test (MMK) (Hamed and Rao, 1998; Daufresne et al., 2009; Zhang et al., 2012) was employed and more detailed algorithm of the MMK can be referred to Daufresne et al. (2009). Based on the MMK (Altman and Bland, 2011) and Sen's slope, trends of MDSI were evaluated and subdivided into seven grades (Table 3).

Table 3 Classification of MDSI-based drought tendencies

$MDSI_{slope}$	$\|Z\|$		
	$\|Z\| \leqslant 1.960$	$1.960 < \|Z\| \leqslant 2.576$	$\|Z\| > 2.576$
Slope<0	Slightly Dry	Dry	Significantly dry
Slope=0		No tendency	
Slope>0	Slightly wet	Wet	Significantly wet

3.4 Hurst exponent

The persistency of MDSI across China was evaluated using the Hurst exponent (Hurst, 1951) based on the rescaled range (R/S) analysis method with respect to long-range correlation. The Hurst exponent ranges from 0 to 1, with H = 0.5 indicating random nature, and H > 0.5 persistent tendency of the current changes. The greater the H value the stronger the persistency of the time series; 0 < H < 0.5 indicates that the future changes are opposite of the past, i.e. the anti-persistency. The smaller the H value the stronger the anti-persistency (Hurst, 1951). According to the Hurst exponent and Sen's slope, the persistency of MDSI was divided into five grades (Table 4). Fig. 2 demonstrates the entire analysis procedure of the current study.

Table 4 Classification of MDSI-based drought persistency

$Slope_{MDSI}$	Hurst		
	Hurst ＜ 0.5	Hurst = 0.5	Hurst ＞ 0.5
$Slope_{MDSI}<0$	From dry to wet 1	No persistency	Persistent drought 2
$Slope_{MDSI}=0$		No persistency	
$Slope_{MDSI}>0$	From wet to dry 3	No persistency	Persistent wetness 4

4. Results

4.1 Applicability of MDSI in drought monitoring across China

4.1.1 Remote sensing DIs vs. SM relations

We evaluated applicability of 9 drought indices in drought monitoring across China (Fig. S1), and found that DIs considering ET and PET, such as CWSI, DSI, and MDSI, had higher correlation coefficients with SM than other DIs. MDSI had higher correlation coefficients with SM than did other DIs. All DIs monitored SM changes in the southwest of SLRB, the YRB, and the northeast of IRB (refer to Fig.1d for the location of major river basins), while MDSI described SM changes better than other DIs at a larger spatial scale. It was also found that relatively poor drought monitoring by DIs in the south of the YZRB and MDSI had high correlation with SM. Furthermore, comparison between CWSI, DSI and MDSI indicated that significant correlation between MDSI (97.92%) and SM was much higher than that between CWSI (46.36%) and DSI (46.04%) in the vegetation coverage area across China (Fig. 3).

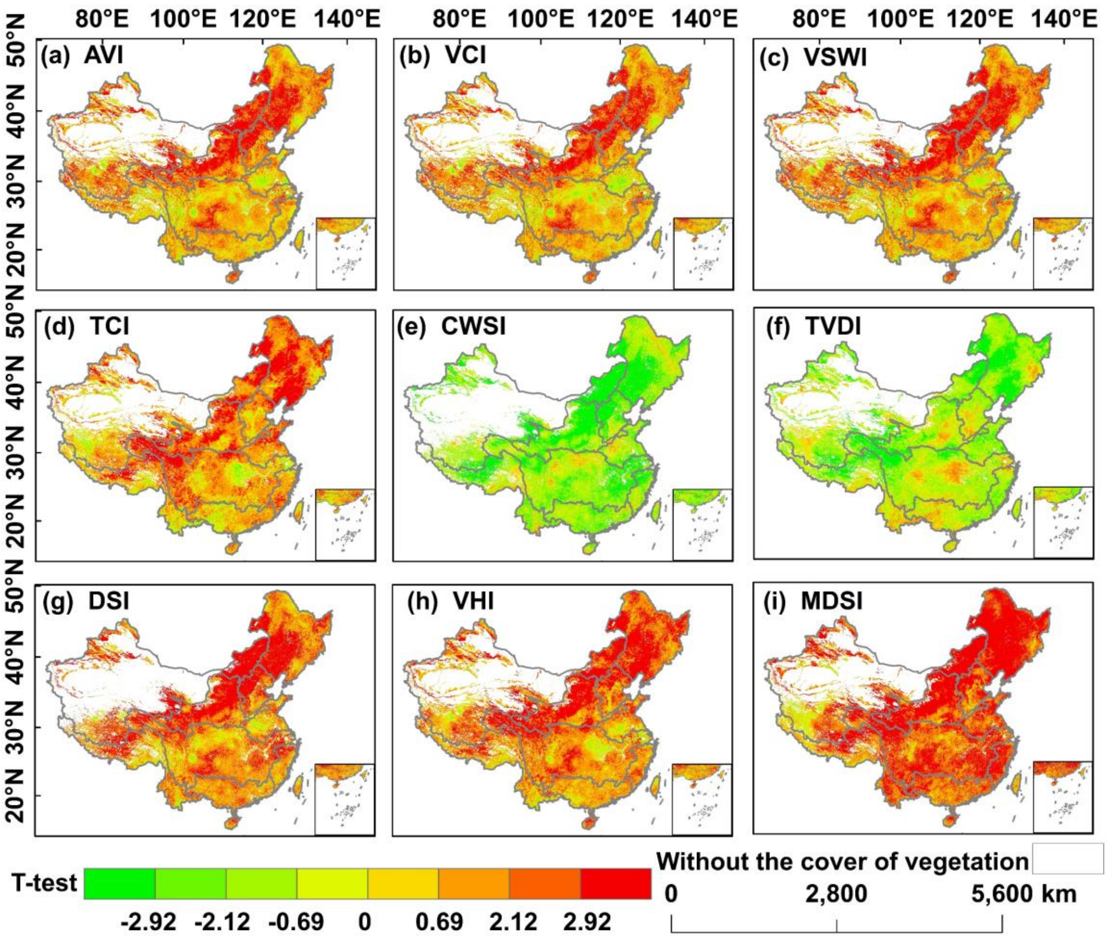

Fig. 3 Spatial distribution of T-test results for correlation coefficients between drought index and SM during the growing season. The critical value of 0.1, 0.05, 0.01 significance level corresponding to t-test are 0.69, 2.12 and 2.92, respectively.

Correlations between DIs and SM for specific river basins across China (Fig. S2) indicated better monitoring performance of MDSI within 9 major river basins (T-test>2.12, p<0.05). Except MDSI, the other DIs poorly monitored SM changes over the HRB, PRB, SWRB, and SERB (T-test value＜2.12, p＞0.05). For areas with different vegetation types (Fig. S3), MDSI monitored well the SM of regions with all vegetation types (T-test>2.12, p<0.05), and especially the SM of the grassland, crops, and Forest (T-test value>2.92, p<0.01). Thus, it was evident that MDSI, compared to other DIs, had monitored SM changes well across China, and deemed to be the right choice for drought monitoring practice.

4.1.2. Remote sensing DIs vs. SPI-3 relations

We quantified relations between DIs and SPI-3 and the significance of correlation was evaluated using the T-test method (Fig. S4). It was found that DIs considering NDVI, such as AVI, VCI, and VSWI, had lower correlation coefficients with SPI-3 than had other DIs. The correlation between DIs and SPI-3 was similar to SM, MDSI had shown advantages over other DIs in terms of its relation with SPI-3 in most phases expected in autumn and growing seasons. The spatial pattern of relations between 9 DIs and SPI-3 during the growing season (Fig. 4) showed that MDSI did better in describing SPI-3 changes than other DIs across China. It is worth noting that MDSI can also effectively monitor drought changes in areas with sparse meteorological observation sites, overcoming the spatial discontinuity of meteorological drought monitoring based on SPI-3, such as the Qinghai-Tibet Plateau and North China. Similar to agricultural drought monitoring, MDSI had relatively satisfactorily monitored meteorological drought in the South of the YZRB. DSI, VHI, and MDSI better reflected the impact of precipitation deficit on agricultural drought compared with other DIs, significantly related stations between MDSI (68.32％) and SPI-3 were much higher than those of DSI (32.35%) and VHI (29.74%) for selected 1957 meteorological stations across China (Fig. 3).

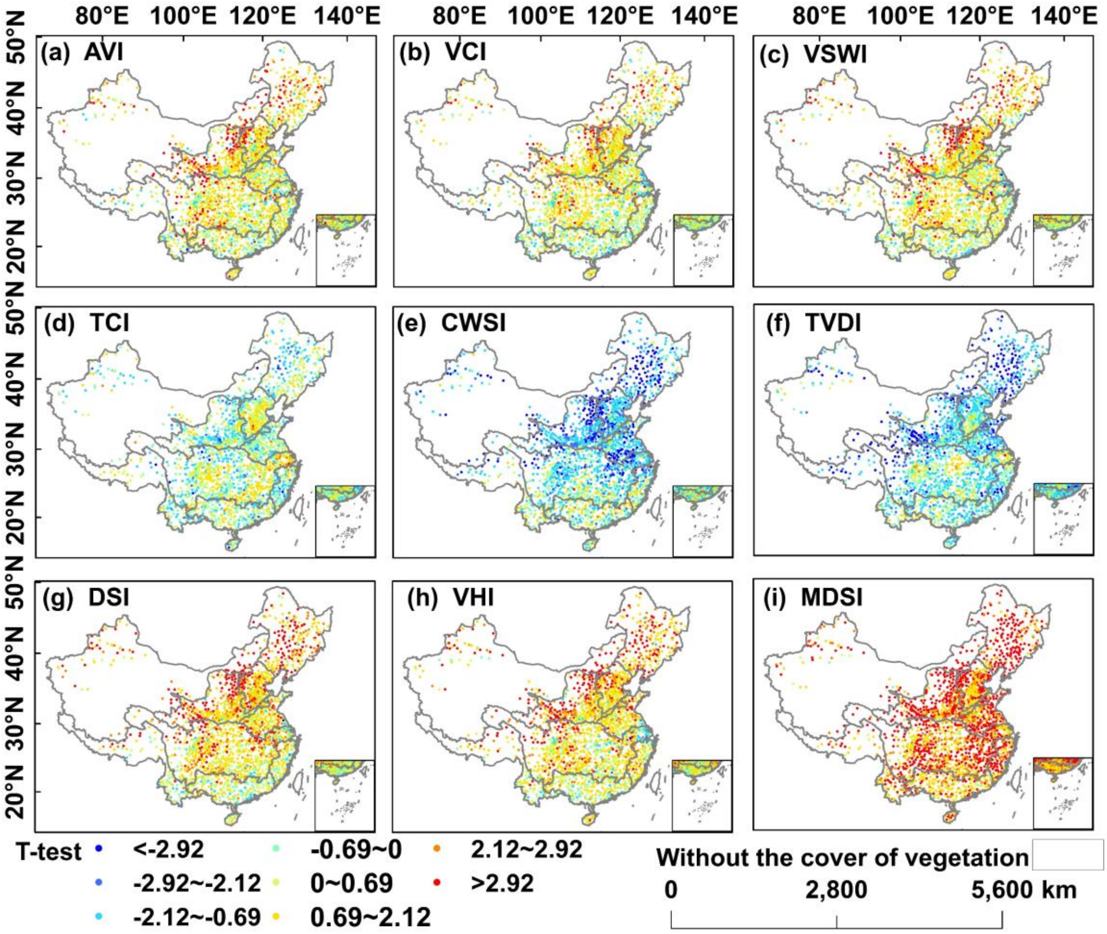

Fig. 4 Spatial distribution of T-test results for correlation coefficients between drought index and SPI-3 during the growing season across China.

For monitoring performance of DIs in different river basins (Fig. S5), MDSI adequately monitored SPI-3 changes in 7 major river basins (T-test value > 2.12, P < 0.05), except PRB and SWRB. However, the meteorological drought monitored by other DIs was more frustrating than MDSI in the PRB and SWRB. For monitoring meteorological drought in regions with different vegetation types (Fig. S6), MDSI monitored the meteorological drought of regions with all vegetation types (T-test>2.12, p<0.05), especially the meteorological drought of the grassland, crops, and Forest (T-test value>2.92, p<0.01). Thus, MDSI had a more widespread and reliable applicability in monitoring meteorological drought across China.

4.1.3 Time lag responses of MDSI and other DIs to SPI-3

We analyzed correlation between DIs and cumulative precipitation at time lags of 0-12 months (Wang et al., 2003). The month of maximum correlation coefficient between drought index of the growing season scale and average SPI-3 in the first 12 months is the lag time. Fig. 5 shows the spatial heterogeneity of lag time in response of DIs to SPI-3 change. We found a considerable lag time in response of agricultural drought to the SPI-3 change. Comparison of lag times in response of DIs to the SPI-3 change indicated that DIs, considering vegetation greenness and canopy temperature (TVDI, VHI, and MDSI) usually had a shorter lag time than other DIs, particularly in YZRB, HURB and PRB. The DIs, which takes into account crop water stress or vegetation greenness (AVI, VCI, VSWI, CWSI and DSI), had a longer lag time in their response to the SPI-3 change, especially in the YRB. Analysis showed that DIs considering onefold factors usually had longer lag time in response to DIs to SPI-3 change. However, the lag time of MDSI (58.25%) and SPI-3 was less than 3 months, which was higher than TVDI (53.45%) and VHI (47.32%) for selected 1957 meteorological stations across China (Fig. 5), indicating that MDSI captured well the agrometeorological drought.

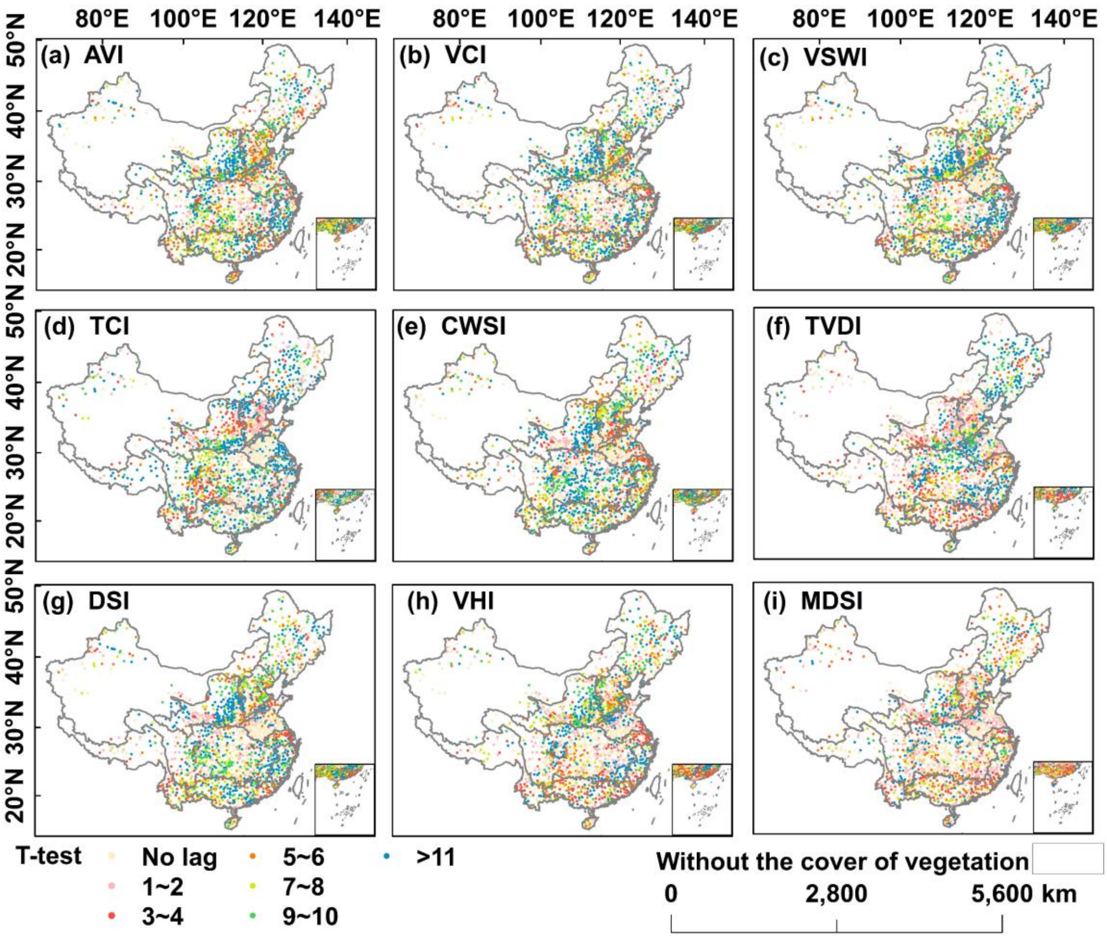

Fig. 5 Spatial distribution of lag time between drought index and SPI-3 during the growing season across China.

It can be seen from Fig 4 and Fig. 6 that the correlation between DIs and SPI-3 during the growing season increased significantly given the consideration of lag time, while the spatial pattern of correlation was similar before and after the consideration of lag time. Given the consideration of lag time, the correlation between SPI-3 and MDSI was still the highest when compared to other DIs, indicating that MDSI better monitored agricultural drought from the viewpoint of meteorological droughts. For correlation between DIs and SPI-3 for different river basins (Figs. S5, S7) and for regions with different vegetation types (Figs. S6, S8), different correlations between drought indices and precipitation were observed. The correlation between DIs and SPI-3 in the YRB, SLRB and IRB increased greatly, which indicated that the lack of precipitation in these basins had a greater impact on the development of agricultural economy. The correlation between DIs and SPI-3 in HURB and HARB was remote, which indicated that the occurrence of agricultural drought in these basins was greatly affected by the precipitation in the same period. From the viewpoint of vegetation types, before and after considering lag time (Figs. S6, S8) impacts on correlations between DIs and SPI-3 were small, indicating that the lag time in response of agricultural drought to precipitation was heavily influenced by the location but not mainly by vegetation type.

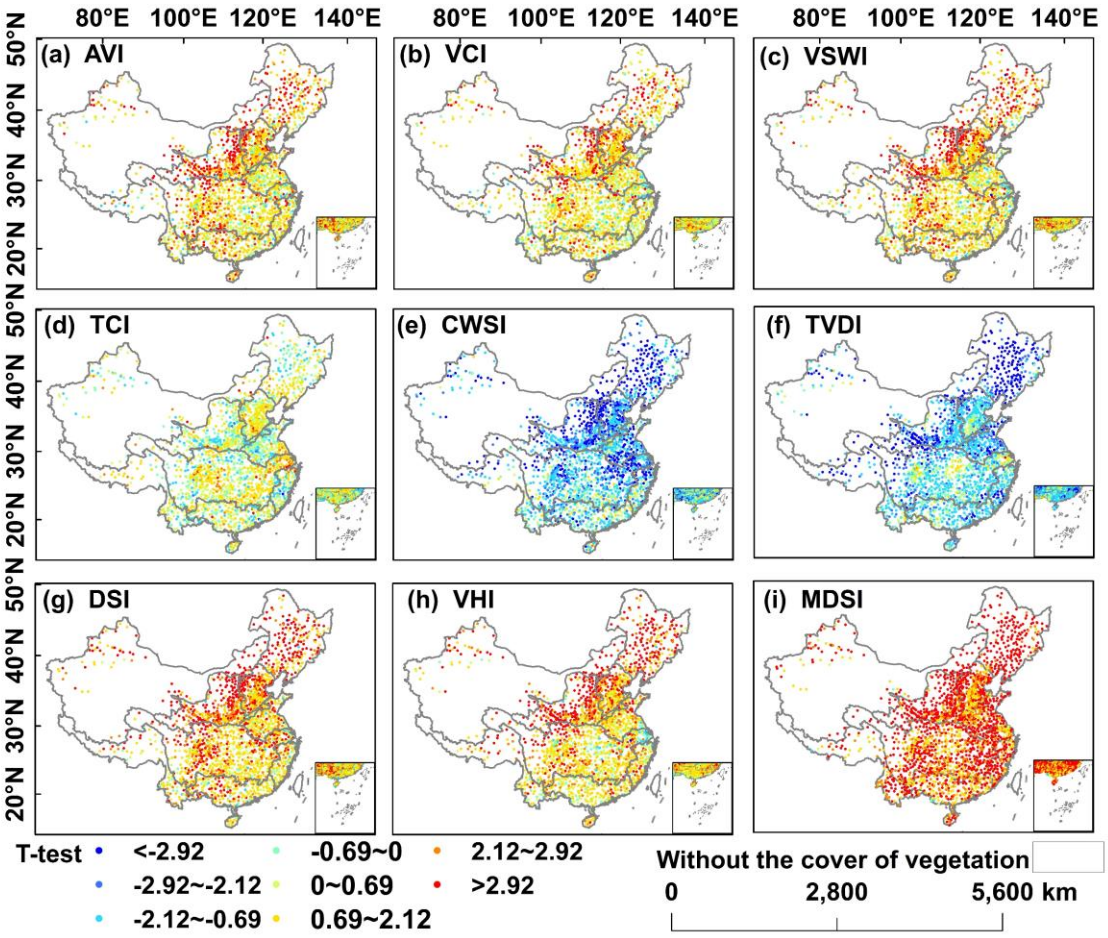

Fig. 6 Spatial distribution of T-test results for correlation coefficients between drought index and SPI-3 during the growing season considering time lag.

Considering the impact of irrigation on agriculture (Yu et al., 2019), we computed maximum correlation coefficients between DIs and SPI-3 for different irrigation areas. It can be seen from Fig. S9 that for different irrigation areas, the maximum correlation coefficients of agricultural drought response to meteorological drought followed the following order, i.e. irrigated-single crop > rainfed crop > irrigated-double crop > irrigated-triple crop. Comparison of the T-test values of the correlation coefficients between MDSI and other DIs and SPI-3 in different irrigation areas after considering the lag time showed that lower drought monitoring performance was observed for drought monitoring indices given irrigated-single crop. Even so, MDSI still showed an advantage over drought indices in monitoring agricultural droughts in different agricultural areas.

4.1.4 Correlation between DIs and drought-affected areas

Previous studies mostly focused on the verification of remote sensing drought indices using SM, precipitation or meteorological drought indices (Sun et al., 2017; Zhang et al., 2018; Jiao et al., 2019; Yu et al., 2019; Li et al., 2020). Correlation coefficients were computed between the drought-affected area of each province from the National Bureau of Statistics and the average of the nine annual-scale DIs (Fig. 7). It can be seen from Fig. 7 that except for TCI and TVDI, drought indices considered in this study successfully monitored agricultural drought-affected area over >50% of the provinces in China, while MDSI monitored well agriculture drought-affected areas in all the provinces. In addition, DSI, VHI, and MDSI monitored the total drought-affected area over 40% of the provinces, while MDSI monitored well the total drought-affected area over >50% of the provinces. Results indicated that MDSI considering greenness and temperature of the vegetation canopy, structure and physiological parameters of vegetation, and water shortage degree of crops better captured crop yields and was of considerable applicability for agricultural drought monitoring.

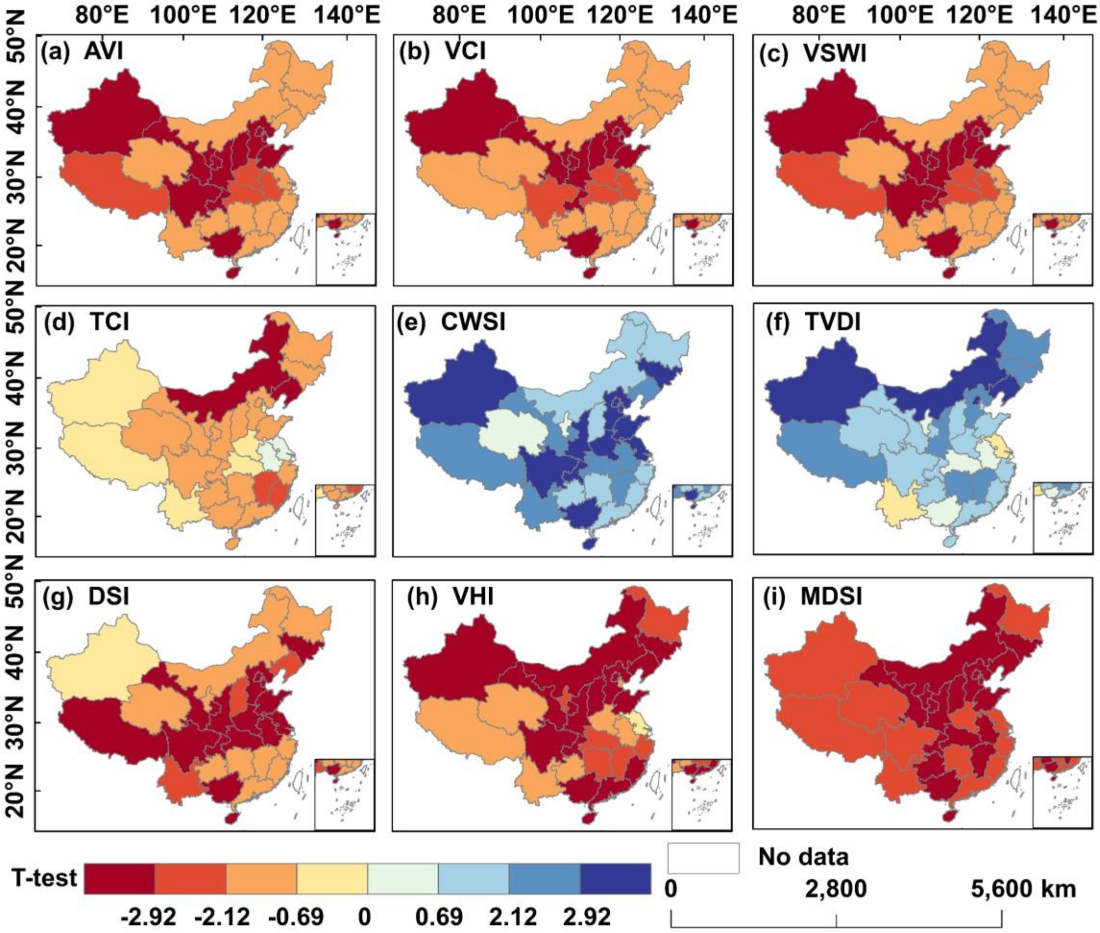

Fig. 7 Spatial distribution of T-test results for correlation coefficients between drought index and total drought-affected area at the annual scale.

4.2 Spatiotemporal pattern of MDSI droughts across China during 2001 to 2018

4.2.1 Temporal changes of annual droughts across China

We analyzed drought changes across China using the MDSI variation within nine river basins and related cumulative anomalies of MDSI. It can be seen from Fig. 8 that an extremely significant wetting tendency was observed in YZRB, YRB, PRB and

SLRB with a long-term trend greater than 0.25 / 10a. Meanwhile, a significant wetting tendency was found in the SERB with long-term trends of 0.27 / 10a. Insignificant wetting tendency was identified in HURB, HARB and SWRB. The cumulative anomalies of MDSI decreased and then increased in the YZRB, the YRB, the PRB, the SLRB and the SERB. Specifically, cumulative anomalies of MDSI reached the trough value in 2009 in the YRB, the SLRB, the IRB and the SERB, indicating that 2009 was the time point for transition from drying to wetting conditions for these basins. Similarly, the transition from drying to wetting conditions in the YZRB and PRB occurred in 2013.

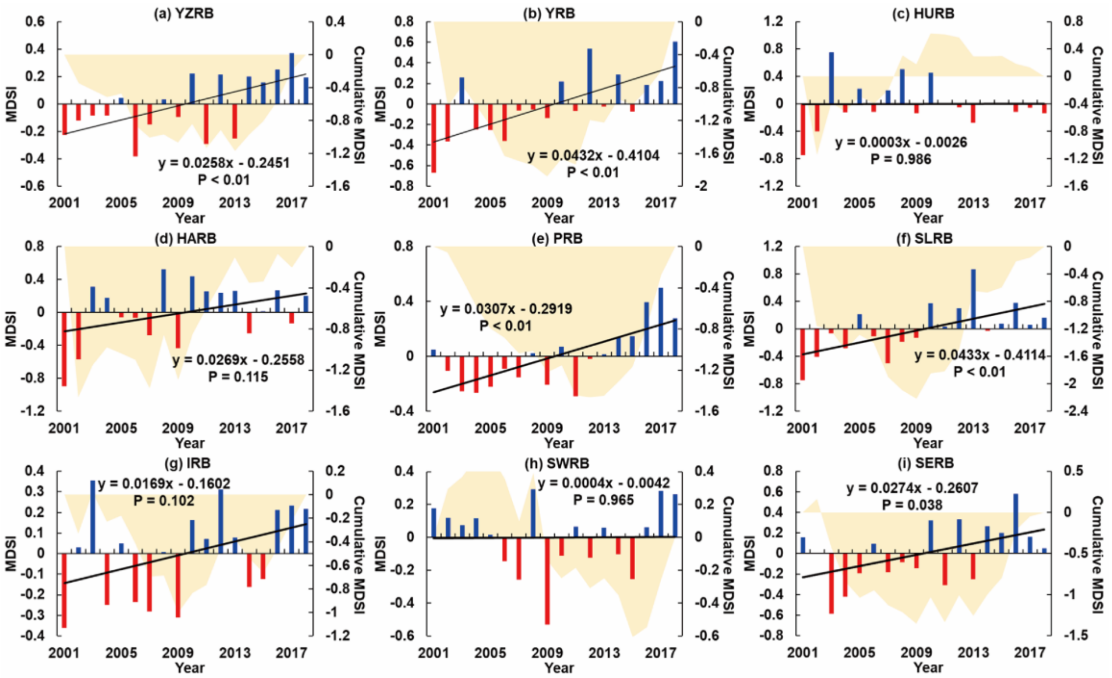

Fig. 8 Annual average MDSI and related cumulative anomalies within 9 major river basins across China during 2001-2018.

4.2.2 Trends of droughts across China

According to Table 3, the change trend of MDSI was divided and the results are shown in Fig. 9. At the monthly scale, a slight drying trend was found in the Xilin Gol grassland in March, and the drying tendency may have a serious impact on the greening of grass. The periods of January to March, and July to August witnessed intensifying droughts over the HURB, particularly for the period from July to August, while the period of July to August was the critical period for summer maize and rice. The period from November to February of the following year witnessed a drying tendency in the hinterland of the Qinghai-Tibet Plateau. A remarkable wetting tendency was found during May to September over middle and upper reaches of the YRB. The period from September to January witnessed a considerable wetting tendency in regions south to the YZRB. The spatial pattern of trends in seasonal droughts was similar to that of monthly droughts. Drought trends during the growing season and at the annual scale were consistent in spatial pattern with the trends of autumn droughts, implying a larger contribution of autumn trends to trends of droughts at the annual scale during the growing season.

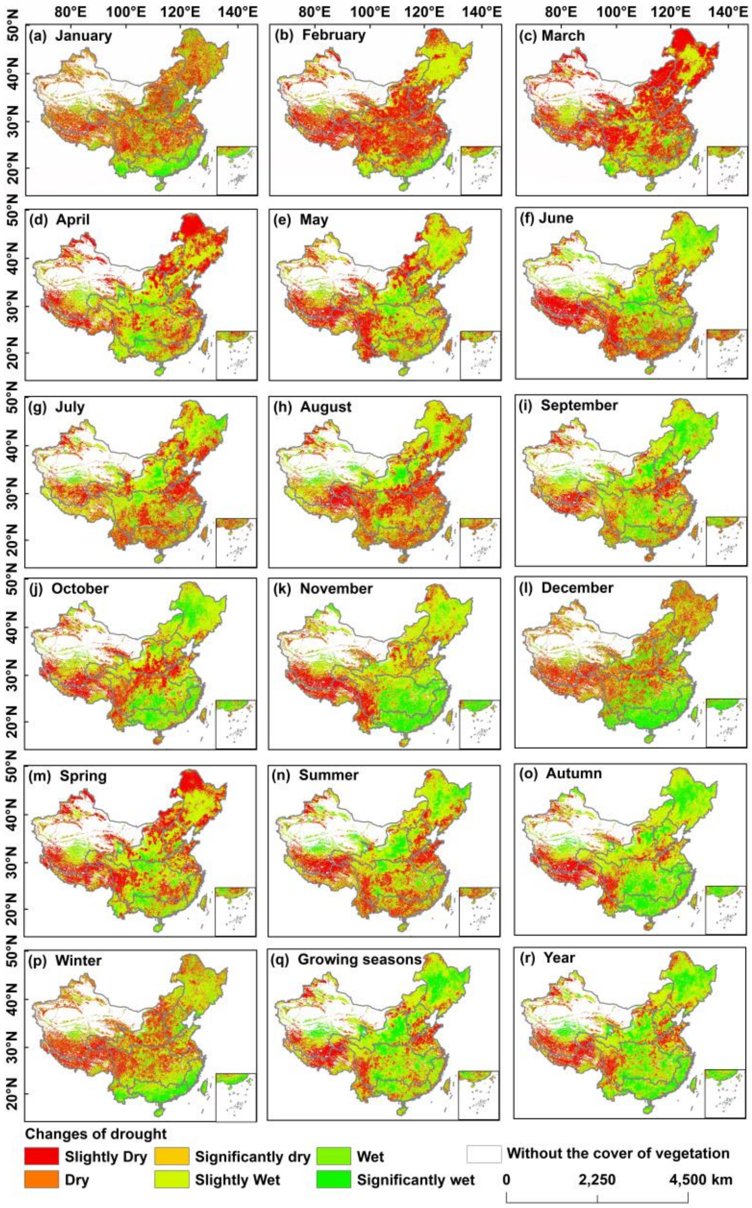

Fig. 9 Spatial pattern of MDSI-based drought tendency at different time scales across China during 2001-2018.

Changes in the underlying surface have an impact on the changing trend of regional drought. We set up four scenarios and control scenarios (unchanged area) according to the spatial distribution of the transformed land use pattern (Fig. 1b), then calculated the average of trends in monthly droughts for five scenarios (Fig. 10).

The trend values of MDSI in the YRB, the HURB and the HARB were significantly higher than those in the unchanged area, showing that ecological restoration helped mitigate droughts (Fig. 10). Nevertheless, the trend of MDSI in the IRB was significantly lower than that in the regions with unchanged area, since the IRB is mostly the pastoral area, and overgrazing leads to further deterioration of the ecological environment (Qiu et al., 2020). For drought trends influenced by urbanization in the YZRB, the YRB, the HARB, the PRB, the SERB, MDSI over the urbanized regions was lower than that over the regions with unchanged area. This result indicates that urbanization can potentially intensify droughts. For the cultivated land reclamation area in the YRB and IRB, the increased irrigation consumption can help mitigate agricultural droughts. In the regions with grassland, degraded grasslands are found mainly in the IRB (Fig. 2b, d), and the intensified drought in turn will enhance grassland degradation and reduce grassland productivity, mainly in the Xilin Gol grasslands in March and in the Qinghai-Tibetan Plateau from November to February.

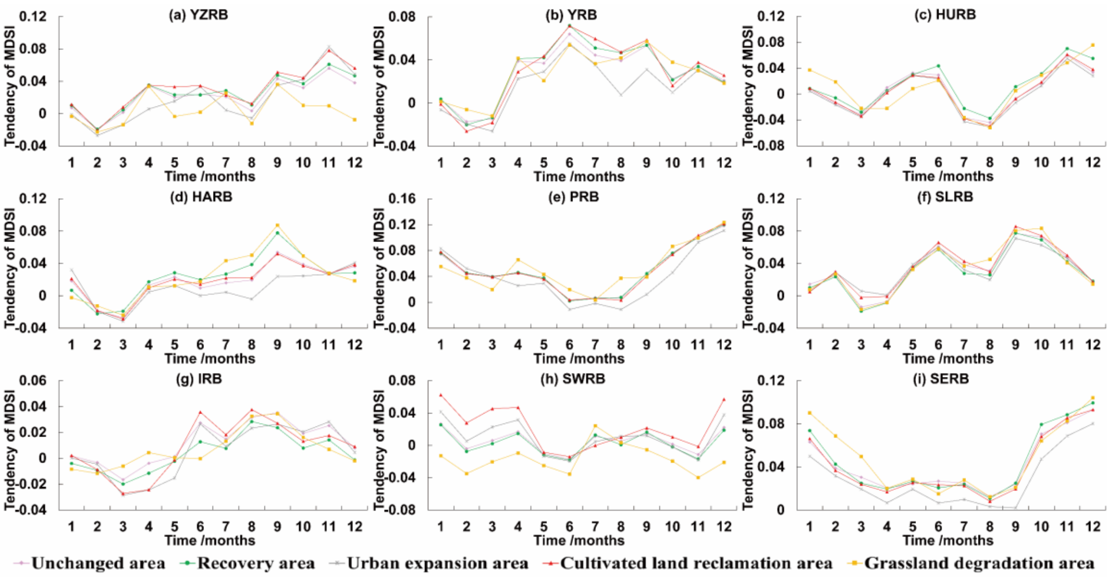

Fig. 10 MDSI-based drought tendency under land use transform at monthly scale.

4.2.3 Persistency of droughts across China

According to Table 3, the change trend of MDSI was divided and the results are shown in Fig. 11. It can be seen from Fig. 11 that general anti-persistency of droughts was observed across China, indicating that the tendency of drought in the near future was opposite to that in the past. At the monthly scale, in the near future, most areas of the Xilin Gol grassland was dominated by a drying tendency from June to February. Meanwhile, the periods of July witnessed a drying tendency in the paddy areas of the HURB and future drought would potentially be intensified. The periods of May to September witnessed intensified droughts in the SLRB and the YRB in the near future. In addition, the seasonal and monthly drought trends had a strong similarity in the spatial distribution, while the spatial pattern of persistency of drought during the growing season and that at the annual scale was more consistent with that of summer drought. Therefore, the persistency of summer drought contributed the most to the persistency of droughts during the growing season and that at the annual scale.

We also analyzed the Hurst exponents of MSDI over five scenarios from 2000 to 2018, showing the impacts of land use changes on drought persistency (Fig. 1b). It can be seen from Fig. 11 that the average value of the Hurst exponent of the nine major river basins in China ranged from 0.40 to 0.50 and droughts within these 9 major river basins generally had weak anti-persistency. The degraded grassland enhanced anti-persistency of drought (mainly referring to IRB). Droughts over the regions with urban expansion areas and cultivated land reclamation areas were subject to weakened anti-persistency to a certain extent. From the Hurst variation range under the five scenarios, indicating that changes in the underlying features of the YZRB, the IRB and the SWRB remarkably modified the persistency of drought.

5 Discussion

Our overall goal was to enhance the accuracy of drought monitoring by developing an MDSI that can be applied across countries with large areas, and it was suitable for areas with sparse stations. A tremendous amount of studies has reached a consensus that constructing drought indices based on univariate or bivariate is likely to be insufficient for accurate drought monitoring (Huang et al., 2015; Chen et al., 2020). In addition, how to effectively integrate different drought-related variables is the key to construct comprehensive drought index. However, previous works mostly used fixed weights to blend different drought-related variables (Rhee et al.,2010; Hao et al., 2015; Sun et al., 2017), which ignored the impact of regional differences on weights. In this study, MDSI was developed based on the constrained optimization method to calculate the assigned weights for inputs at multi-temporal scales to reflect the agricultural drought information, and verified its applicability at the national level (Figs. 3, 4, 7). In general, NDVI-based DIs poorly monitored droughts in southern China where forests and crops were dominant with abundant precipitation and strong vegetation transpiration (Li et al., 2017). However, NDVI constructed by the visible light and near-infrared monitored the health of vegetation through chlorophyll content, but could not provide timely information about energy and water exchange among vegetation, soil, and atmosphere (Olsen et al., 2015). In addition, previous works have confirmed that there is a strong linear relationship between NDVI and LAI (Fensholt et al., 2004; Qiao et al., 2019), but some studies show that the impact of climate change on NDVI and LAI has a certain degree of difference (Myneni et al., 2007; Lee et al., 2013), and there is the spatial heterogeneity in the impact of LAI change on terrestrial water storage in China (Tao et al., 2020). Given the limitation of DSI when used for drought monitoring at a large scale with complex underlying surface, MDSI combines multiple vegetation growth limiting factors, thereby leading to the best performance among DIs.

Xu et al. (2018) found that the response of vegetation index to long-term drought was mainly in Northeast China and YRB, which is similar to our results, as shown in Fig. 5. The main reason is that afforestation caused high water holding capacity of the soil and short-term increase or decrease of precipitation could not trigger significant SM changes in YRB, while the northeastern and southern coastal areas of the SLRB are dominated by woodlands and shrubs. Higher vegetation coverage and relative stable ecological environment caused lower responses of DIs to precipitation changes (He et al., 2017). However, the lag response of DIs for a long time to meteorological drought makes it difficult to assess the impact of insufficient precipitation on vegetation, while MDSI has greatly improved in this aspect.

Some researchers have focused on the spatial-temporal distribution of drought in China, based on the meteorological station data or remote sensing drought index. Using the Palmer Drought Severity Index, Yan et al. (2016) found that an extreme drought event occurred in 2001, and relatively severe droughts occurred in North China, which is similar to our results shown in Fig. 8. The main reason is that the strong La Niña phenomenon occurred in 2000-2001, which led to the abundant precipitation in the South and the dry precipitation in the north (Li et al., 2019). In addition, based on the

Integrated Surface Drought Index (ISDI) and modified Temperature Vegetation Drought Index (mTVDI), Zhou et al. (2017) and Zhao et al. (2017) found that drought in Northeast China and the south of the YZRB showed an obvious decreasing trend in different periods. Zhu et al. (2019) showed that the SM of farmland increased fastest in summer and autumn. Many studies above have focused on the temporal-spatial pattern of drought across the China, while there is comparability in the temporal-spatial pattern of drought across the China between this study and previous studies.

The results of the study demonstrated that ecological restoration helped mitigate droughts in Huang-Huai-Hai Plain, and a remarkable wetting tendency was found during May to September in the middle and upper reaches of the YRB. Ye et al. (2019) confirmed that ecological restoration has a negative impact on SM in humid and semi-humid areas, while it has a positive impact on SM in arid and semi-arid areas. Under the influence of China's widespread greening, summer precipitation increased in the Huang-Huai-Hai Plain (Yu et al., 2020). However, some studies also showed that ecological restoration reduced SM (Feng et al., 2017; Li et al., 2018). These results suggest that if vegetation greening leads to reduced SM, MDSI can overestimate the increase of soil wetness in response to ecological restoration across China. In addition, urbanized areas have a potentially negative effect on drought mitigation. These areas are urbanizing rapidly, and the rate of urban expansion exceeds the capacity of the ecological environment, leading to the contradiction between people and land (Liao et al., 2020).

Our study made an improvement of Drought Severity Index (DSI), and the results could provide references for the development of agricultural drought in China and China's food security. In this study, the relationship between in-situ drought index (SPEI-3) and several factors limiting vegetation growth was considered. Compared with the application of SPEI-3 limited to regions with available meteorological ground observations, establishing reliable integrated remote sensing based agricultural drought-related variables which could be applied in various environmental regions without relying on ground observations was an important avenue for future work (Ayantobo et al., 2017; Liu et al., 2019; Jiao et al., 2019). Also, in-situ observations of meteorological variables cannot completely reflect areal drought characteristics (Sun et al., 2017). In addition, MDSI has higher spatial resolution than reanalysis data, allowing for high spatial resolution agricultural and meteorological drought monitoring. However, the accuracy of drought monitoring is still affected by terrain, snow cover, soil water holding capacity, and human activities, which is also the main reason for the unsatisfactory monitoring in a few areas. In addition, the Hurst exponent is also used to study the persistency of drought, but the prediction of future drought has great uncertainty. In further studies we will consider the influence of other factors on the accuracy of drought monitoring, and try to use a variety of methods to evaluate the future trend of drought.

6 Conclusion

In this study, MDSI with vegetation greenness, crop water shortage, canopy temperature, vegetation structure and physiological status as input variables was constructed. We compared DI and MDSI with SM, precipitation, and drought-affected area in order to evaluate drought monitoring by, evidencing the applicability of MDSI in drought monitoring across China. Based on MDSI, we analyzed droughts across China in both space and time. The main conclusions can be drawn as follows:

(1) MDSI described SM changes at a larger spatial scale better than other DIs, especially in south of the YZRB it has been significantly improved. At most time scales, MDSI had a higher correlation coefficient with SM/SPI-3 than other DIs, and had highest correlation in agricultural regions, indicating that MDSI had remarkable advantages over DIs in monitoring agricultural droughts. Besides, MDSI can monitor well drought-affected areas, further corroborating the applicability of MDSI in agricultural drought monitoring across China.

(2) The nine major river basins in China showed a wetting tendency during 2001-2018, especially in the YZRB, YRB, PRB and SLRB. Xilin Gol Grasslands underwent a drying tendency in March. A wetting tendency can be found mainly in the regions south of the YZRB during September to January. Droughts across most regions of China are subject to anti-persistency, showing a drought tendency in the near future may be opposite of the past.

(3) The relationship between drought trends and changes in the underlying surface showed that grassland degradation in IRB intensified drought and enhanced anti-persistency of drought. The ecological restoration in the Huang-Huai-Hai Plain decreased drought risks. Rapid urbanization can potentially intensify droughts, while the cultivated land reclamation areas of the YRB and IRB have promoted drought

alleviation.

(4) Degraded grassland enhanced anti-persistency of drought (mainly refer to IRB). Droughts over the regions with urban expansion areas and cultivated land reclamation areas were subject to weakened anti-persistency. From the Hurst variation range under the five scenarios, drought persistency of the YZRB, the IRB and the SWRB is most affected by the change of underlying features.

Acknowledgments: This research has been supported by the China National Key R&D Program, Grant No. 2019YFA0606900; the Nature Science Foundation for Excellent Young Scholars of Anhui, Grant No. 2108085Y13; Key Research and Development Program Project of Anhui province, China, Grant No. 2022m07020011; The University Synergy Innovation Program of Anhui Province, Grant No. GXXT-2021-048. All authors declare no conflict of interest. The last but not the least, here we would like to express our cordial gratitude to the editor, Prof. Dr. Emmanouil Anagnostou, and anonymous reviewers for their professional and pertinent comments which are greatly helpful for further quality improvement of this manuscript.

References

Agutu, N.O., Aange, J.L., Zerihu,A., et al. (2017). Assessing multi-satellite remote sensing, reanalysis, and land surface models' products in characterizing agricultural drought in East Africa. *Remote Sensing of Environment,2017*(194):287-302.

Allen, M. R., Ingram, W. J. (2002). Constraints on future changes in climate and the hydrologic cycle. *Nature, 419*(6903), 224-232.

Allen, R.G., Pereira, L.S., Raes, D., Smith, M. (1998). Crop Evapotranspiration: Guidelinse for Computing Crop Water Requirements. Fao Irrigation and Drainage Paper 56; FAO-Food and Agriculture Organization of the United Nations Rome: Rome, Italy.

Allen, R., Irmak, A., Trezza, R., Hendrickx, J.M.H., Bastiaanssen, W., Kjaersgaard, J. (2011). Satellite-based ET estimation in agriculture using SEBAL and METRIC. *Hydrological Processes, 26*(25), 4011-4027.

Altman, DG., Bland, J.M. (2011). How to obtain the P value from a confidence interval. *British Medical Journal, 343*(8), d2304, doi: 10.1136/bmj.d2304.

Ayantobo, O.O., Li, Y., Song, S., Yao, N. (2017). Spatial Comparability of Drought Characteristics and Related Return Periods in Mainland China Over 1961–2013. *Journal of Hydrology. 550*, 549–567.

Battisti, D. S., Naylor, R. L. (2009). Historical warnings of future food insecurity with unprecedented seasonal heat. *Science, 323*(5911), 240-244.

Bokusheva, R., Kogan, F., Vitkovskaya, I., Conradt, S., Batyrbayeva, M. (2016). Satellite-based vegetation health indices as a criteria for insuring against drought-related yield losses. *Agricultural & Forest Meteorology, 220*, 200-206.

Carlson, T.N., Gillies, R.R., Perry, E.M. (1994). A method to make use of thermal infrared temperature and NDVI measurements to infer surface soil water content and fractional vegetation cover. *Remote Sensing Reviews, 9*(1-2), 161-173.

Chen, W.Y., Xiao, Q.G., Sheng, Y.W. (1994). Application of anomaly vegetation index to monitoring heavy drought in 1992. *Journal of Remote Sensing, 1994*(2), 106-112.

Chen, S., Zhong, W.S., Pan, S.H., Xie, Q.J., Kim, T.W. (2020). Comprehensive Drought Assessment Using a Modified Composite Drought index: A Case Study in Hubei Province, China. *Water, 12*, 462-473.

Coats, S., & Mankin, J.S. (2016). The challenge of accurately quantifying future megadrought risk in the American Southwest. *Geophysical Research Letters, 43*, 9225–9233.

Cooke, W.H, Mostovoy, G.V., Anantharaj, V.G., Jolly, W.M. (2012). Wildfire Potential Mapping over the State of Mississippi: A Land Surface Modeling Approach. *Giscience & Remote Sensing, 49*(4), 492-509.

Cui, L., L. Wang, S. Qu, R.P. Singh, Z. Lai, R. Yao. (2019). Spatiotemporal extremes of temperature and precipitation during 1960-2015 in the Yangtze River Basin (China) and impacts on vegetation dynamics. *Theoretical & Applied Climatology, 692*, 675-692.

Daufresne, M., K. Lengfellner, U. Sommer. (2009). Global warming benefits the small in aquatic ecosystems. Proc. *Natl. Acad. Sci. U.S.A., 106*(31), 12788–12793.

Dirmeyer, P.A., Guo, Z., Gao, X. (2004). Comparison, validation, and transferability of eight multiyear global soil wetness products. *Journal of Hydrometeorol, 5,* 1011–1033.

Fan, Y., van den Dool, H. (2004). Climate Prediction Centre (CPC) global monthly soil moisture data set at 0.5° resolution for 1948 to present. *Journal of Geophysical Research Atmospheres, 2004,* 109.

Feng, X., Li, J., Cheng, W., Fu, B., Wang, Y., Lü, Y. (2017). Evaluation of AMSR-E retrieval by detecting soil moisture decrease following massive dryland re-vegetation in the Loess Plateau, China[J]. *Remote Sensing of Environment, 196,* 253-264.

Fensholt R, Sandholt I, Rasmussen M S. (2004). Evaluation of MODIS LAI, fAPAR and the relation between fAPAR and NDVI in a semi-arid environment using in situ measurements[J]. Remote Sensing of Environment, 91(3-4):490-507.

Fisher, R., Williams M., COSTA D. (2007). The response of an Eastern Amazonian rain forest to drought stress: results and modelling analyses from a throughfall exclusion experiment. *Global Change Biology, 13(11)*, 2361-2378.

Hamed, K.H., A.R. Rao. (1998). A modified Mann-Kendall trend test for autocorrelated data. *Journal of Hydrology, 204*, 182-196.

Hao, C., Zhang, J., Yao, F. (2015). Combination of multi-sensor remote sensing data for drought monitoring over Southwest China. *International Journal of Applied Earth Observations & Geoinformation, 35*, 270-283.

He, H., Li, H., Zhu, J., Yang, Y., Wei, Y., Li, Y.(2017). Soil Water-holding Capacity under the Condition of Fencing in Alpine Meadow of the Source Region of Yellow River. *Chinese Journal of Grassland, 39*(5), 62-67 (in Chinese with English abstract).

He, X., Wada, Y., Wanders, N., Sheffield, J. (2017). Human water management intensifies hydrological drought in California. *Geophysical Research Letters*, 1-19. Doi:10.1002/2016GL071665.

Huang, J., Zhuo, W., Li, Y., Huang, R., Sedano, F., Su, W., Dong, J., Tian, L., Huang, Y., Zhu, D. (2018). Comparison of three remotely sensed drought indices for assessing the impact of drought on winter wheat yield. *International Journal of Digital Earth, 2018*, 1-23.

Huang, S.Z., Huang, Q., Chang, J.X., Zhu, Y.L., Leng, G.Y., Xing, L. (2015). Drought structure based on a nonparametric multivariate standardized drought index across the Yellow River basin, China. *Journal of Hydrology. 530*, 127–136.

Hu, P., Zhang, Q., Shi, P., Chen, B., Fang, J.(2018). Flood-induced mortality across the globe: Spatiotemporal pattern and influencing factors. *Science of The Total Environment, 643*, 171-182.

Huete, A.R.(1988). A soil-adjusted vegetation index (SAVI). *Remote Sensing of Environment, 25*(3), 295–309.

Hurst, H.E.(1951). Long-term storage capacity of reservoirs. *Transactions of the American Society of Civil Engineers, 116*(1), 770-799.

Jackson, R.D., Idso, S.B., Reginato, R.J., P.J. Pinter Jr. (1981). Canopy temperature as a crop water stress indicator. *Water Resources Research, 17*(4), 1133-1138.

Jackson, R.D., Kustas, W.P., Choudhury, B.(1988). A re-examination of the crop water stress index. *Irrigation Science, 9*(4), 309-317.

Jiao, W., Tian, C., Novick, K.A., Chang, Q. (2019). A new station-enabled multi-sensor integrated index for drought monitoring. *Journal of Hydrology, 574*, 74-85.

Kapoor, D., Bhardwaj, S., Landi, M., Sharma, A. (2020). The impact of drought in plant metabolism: how to exploit tolerance mechanisms to increase crop production. *Applied Sciences, 10*(16), 5692.

Kogan, F. (2012). Global drought watch from space at work: Crop losses and food security. *American Geophysical Union, 78*(4), 621-636.

Kogan, F., Salazar, L., Roytman, L. (2012). Forecasting crop production using satellite-based vegetation health indices in Kansas, USA. *International Journal of Remote Sensing, 33*(9-10), 2798-2814.

Kogan, F.N. (1995). Application of vegetation index and brightness temperature for drought detection. *Advances in Space Research, 15*(11), 91-100.

Kogan, F.N. (1995). Droughts of the late 1980s in the United States as derived from NOAA polar-orbiting satellite data. *Bull. Amer. Meteor. Soc., 76*(5), 655-668.

Lee, J.E., Frankenberg, C., Van, D.T.C., Berry, J.A., Guanter, L., Boyce, C.K., Fisher, J.B., Morrow, E., Worden, J.R., Asefi, S. (2013). Forest productivity and water stress in Amazonia: observations from GOSAT chlorophyll fluorescence. *Proceedings of the Royal Society B: Biological Sciences, 280(1761)*, 176-188.

Liao, S., Wu, Y., Wong, S. W., Shen, L. (2020). Provincial perspective analysis on the coordination between urbanization growth and resource environment carrying capacity (RECC) in China. *Science of The Total Environment, 730*, 138964.

Li, G., Zhang, F.M., Jing, Y.S., Liu, Y.B., Sun, G. (2017). Response of evapotranspiration to changes in land use and land cover and climate in China during 2001–2013. *Science of The Total Environment, 596-597*, 256-265.

Li, J., Zhang, Q., Chen, Y. D., Singh, V. P. (2015). Future joint probability behaviors of precipitation extremes across China: spatiotemporal patterns and implications for flood and drought hazards. *Global and Planetary Change, 124,* 107-122.

Liu, S., Zamanian, K., Schleuss, P.-M., Zarebanadkouki, M., Kuzyakov, Y. (2018). Degradation of Tibetan grasslands: Consequences for carbon and nutrient cycles. *Agriculture, Ecosystems & Environment, 252,* 93–104.

Li, X., Lu, H., Le, Y., Yang, K. (2018). Comparison of the Spatial Characteristics of Four Remotely Sensed Leaf Area Index Products over China: Direct Validation and Relative Uncertainties. *Remote Sensing, 10(2),* 148-173.

Li, X., Lu, H., Lyu,H. (2017). A Newly Global Drought Index Product Basing on Remotely Sensed Leaf Area Index Percentile Using Severity-Area-Duration Algorithm. *Egu General Assembly Conference*. EGU General Assembly Conference Abstracts.

Li, Y., Strapasson, A., Rojas, O. (2019). Assessment of El Niño and La Niña impacts on China: Enhancing the Early Warning System on Food and Agriculture. *Weather and Climate Extremes*, *27,* 100208.

Li, Z., Han, Y., Hao, T. (2020). Assessing the Consistency of Remotely Sensed Multiple Drought Indices for Monitoring Drought Phenomena in Continental China. *IEEE Transactions on Geoscience and Remote Sensing, 99*, 1-13.

Ma, Z.C., Sun, P., Zhang, Q., Hu, Y.-Q., Jiang, W. (2021). Characterization and Evaluation of MODIS-Derived Crop Water Stress Index (CWSI) for Monitoring Drought from 2001 to 2017 over Inner Mongolia. *Sustainability, 13*(2), 916-932.

McKee, T.B., Doesken, N.J., Kleist, J. (1993). The Relationship of Drought Frequency and Duration to Time Scales. In Proceedings of the 8th Conference on Applied Climatology, Anaheim, CA, USA, 17–22.

Mishra, A. K. Singh, V. P. (2010). A review of drought concepts. *Journal of Hydrology, 391*(1-2), 202-216.

Mu, Q.Z., Zhao, M.S., Kimball, J.S., McDowell, N.G., Running, S.W. (2013). A remotely sensed global terrestrial drought severity index. *Bulletin of the American Meteorological Society, 94*(1), 83-98.

Myneni, R.B., Yang, W., Nemani, R.R., Huete, A.R., Salomonson, V.V. (2007). Large seasonal swings in leaf area of Amazon rainforests[J]. Proceedings of the National Academy of Sciences, 104(12), 4820-4823.

Olsen, J.L., Stisen, S., Proud, R.S., Fensholt, R. (2015). Evaluating EO-based canopy water stress from seasonally detrended NDVI and SIWSI with modeled evapotranspiration in the Senegal River Basin, *Remote Sensing of Environment, 159*, 57-69.

Park, S., Im, J., Jang, E., Rhee, J. (2016). Drought assessment and monitoring through blending of multi-sensor indices using machine learning approaches for different climate regions. *Agricultural & Forest Meteorology, 216*, 157-169.

Liu, Q., Zhang, S., Zhang, H, Bai, Y., Zhang, J. (2019). Monitoring drought using composite drought indices based on remote sensing. *Science of The Total Environment, 711,* 134585.

Li, Y., Piao, S, Li, L.Z.X, Chen, A., Wang, X., Ciais, P., Huang, L., Lian, X., Peng, S., Zeng, Z., Wang, K., Zhou, L. (2018). Divergent hydrological response to large-scale afforestation and vegetation greening in China. *Science Advances, 4, 4182.*

Powell, M.J. (1978). A fast algorithm for nonlinearly constrained optimization calculations. *In: Numerical Analysis. Springer, Berlin, Heidelberg, pp*. 144–157.

Pradhan, P., Costa, L., Rybski, D., Lucht, W., & Kropp, J. P. (2017). A systematic study of Sustainable Development Goal (SDG) interactions. *Earth's Future, 5*(11), 1169-

1179.Sandholt, I., Rasmussen, K., Andersen, J. (2002). A simple interpretation of the surface temperature/vegetation index space for assessment of surface moisture status. *Remote Sensing of Environment, 79(2)*, 213-224.

Qiao, K., Zhu, W., Xie, Z., Li, P. (2019). Estimating the Seasonal Dynamics of the Leaf Area Index Using Piecewise LAI-VI Relationships Based on Phenophases. *Remote Sensing, 11(6),* 689-704.

Qiu, H., Su, L., Feng, X., Tang, J., 2020. Role of monitoring in environmental regulation: An empirical analysis of grazing restrictions in pastoral China. *Environmental Science & Policy*, 114, 295-304

Rhee, J., Im, J., Carbone, G.J. (2010). Monitoring agricultural drought for arid and humid regions using multi-sensor remote sensing data. *Remote Sensing of Environment, 114 (12)*, 2875–2887.

Shen, Z.X, Zhang, Q., Singh, V.P., Pokhrel, Y., Li, J.P., Xu, C.Y., Wu, W.H., 2022. Drying in the low-latitude Atlantic Ocean contributed to terrestrial water storage depletion across Eurasia. *Nature Communications,* 13, 1849. https://doi.org/10.1038/s41467-022-29544-6

Sun, P., Q. Zhang, Q. Wen, V.P. Singh, P. Shi. (2017). Multisource data based integrated agricultural drought monitoring in the Huai River basin, China. *Journal of Geophysical Research, 122*, 10751-10772.

Tao, F.L., Chen, Y., Fu, B.J. (2020). Impacts of climate and vegetation leaf area index changes on global terrestrial water storage from 2002 to 2016. Science of the Total Environment, 724(7), 138298.

Theil, H. (1992). A rank-invariant method of linear and polynomial regression analysis. *Nederl. Akad. Wetensch. Proc., 12*(2), 345-381.

Um, M.-J., Kim, Y., Park, D. (2018). Evaluation and modification of the Drought Severity Index (DSI) in East Asia. *Remote Sensing of Environment, 209*, 66-76.

Vicente-Serrano, S.M., Beguería, S., López-Moreno, J.I., Marta, A.M. (2010). A multiscalar drought index sensitive to global warming: The standardized precipitation evapotranspiration index. *Journal of Climate, 23,* 1696–1718.

Wang, J., Rich, P.M., Price, K.P. (2003). Temporal responses of NDVI to precipitation and temperature in the central Great Plains, USA. *International Journal of Remote Sensing, 24*(11), 2345-2364.

Wilhite, D. A. (2000). Drought as a natural hazard: concepts and definitions. *Drought: A Global Assessment, Vol. I, chapter 1*, 3-18.

Wu, F., Wang, C., Jiang, S.F., Zhang, H., Zhang, B. (2015). Land Degradation Assessment Using Residual Trend Analysis of GIMMS NDVI3g, Soil Moisture and Rainfall in Sub-Saharan West Africa from 1982 to 2012. *Remote Sensing, 7(5),* 5471-5494.

Xu, K., Yang, D., Yang, H., Li, Z., Qin, Y., Shen, Y. (2015). Spatio-Temporal Variation of Drought in China During 1961–2012: A Climatic Perspective. *Journal of hydrology, 526,* 253–264.

Yan, H., Wang, S.Q., Wang, B.J., Lu, H.Q., Guo, A.H., Zhu, Z.C., Myneni, R.B., Shugart, H.H. (2016). Assessing spatiotemporal variation of drought in China and its impact on agriculture during 1982–2011 by using PDSI indices and agriculture drought survey data. *Journal of Geophysical Research: Atmospheres, 121*(5), 2283–2298.

Yazdani, F., Allahdadi, I., Akbari, G.A. (2007). Impact of superabsorbent polymer on yield and growth analysis of soybean (Glycine max L.) under drought stress condition. *Pak J Biol Sci, 10(23)*, 4190-4196.

Ye, L., Fang, L., Shi.Z, Deng, L., Tan, W. (2019). Spatio-temporal dynamics of soil moisture driven by 'Grain for Green' program on the Loess Plateau, China. *Agriculture Ecosystems & Environment, 269,* 204-214.

Ye, L., Shi, K., Zhang, H., Xin, Z., Hu, J., Zhang, C. (2019). Spatio-Temporal Analysis of Drought Indicated by SPEI over Northeastern China. *Water, 11,* 908.

Yu, L., Liu, Y., Liu, T., Yan, F. (2020). Impact of recent vegetation greening on temperature and precipitation over China. *Agricultural and Forest Meteorology, 295*, 108197.

Yu, M., Li, Q., Hayes, M.J., Svoboda, M.D., Heim, R.R. (2014). Are droughts becoming more frequent or severe in China based on the standardized precipitation evapotranspiration index: 1951–2010. *International Journal Of Climatology, 34,* 545–558.

Yu, Q., Zhang, Q., Xu, C.-Y., Du, J., Sun, P., Hu, P. (2019). Modified Palmer Drought Severity Index: model improvement and application. *Environment International, 130*, 104951.

Zargar, A., Sadiq, R., Naser, B., Khan, F. I. (2011). A review of drought indices. *Environmental Reviews, 19*, 333-349.

Zhang, M., & Yuan, X. (2020). Rapid reduction in ecosystem productivity caused by flash drought based on decade-long FLUXNET observations. *Hydrology and Earth System Sciences, 24*, 5579-5593. https://doi.org/10.5194/hess-2020-185

Zhang, Q., Gu, X., Singh, V. P., Kong, D., Chen, X. (2015). Spatiotemporal behavior of floods and droughts and their impacts on agriculture in China. *Global and Planetary Change, 131*, 63-72.

Zhang, Q., H. Yu, P. Sun, V.P. Singh, P. Shi. (2019). Multisource data based agricultural drought monitoring and agricultural loss in China. *Global and Planetary Change, 172*, 298-306.

Zhang, Q., J. Li, V.P. Singh, M. Xiao. (2013). Spatio-temporal relations between temperature and precipitation regimes: Implications for temperature-induced changes in the hydrological cycle. *Global and Planetary Change, 111*, 57-76.

Zhang, Q., Q. Li, V.P. Singh, P. Shi, Q. Huang, P. Sun. (2018). Nonparametric integrated agrometeorological drought monitoring: model development and application. *Journal of Geophysical Research, 123*, 73-88.

Zhang, Q., V.P. Singh, J. Peng, Y.D. Chen, J. Li. (2012). Spatial-temporal changes of precipitation structure across the Pearl River basin, China. *Journal of Hydrology, 440-441*, 113-122.

Zhang, X., Qiu, J., Leng, G., Yang, Y., Gao, Q., Fan, Y., Luo, J. (2018). The Potential Utility of Satellite Soil Moisture Retrievals for Detecting Irrigation Patterns in China. *Water, 10*(11), 1505.

Zhang, X.Q, Yamaguchi, Y. (2014). Characterization and evaluation of MODIS-derived Drought Severity Index (DSI) for monitoring the 2009/2010 drought over southwestern China. *Natural Hazards, 74*(3), 2129-2145.

Zhang, Q., Fan, K., Singh, V.P., Sun, P., Shi, P. (2018). Evaluation of remotely sensed and reanalysis soil moisture against in-situ observations on the Himalayan-Tibetan

Plateau. *Journal of Geophysical Research, 123*, 7132-7148.

Zhao, S.H., Cong, D.M., He, K.X., Yang, H., Qin, Z.H. (2017). Spatial-Temporal Variation of Drought in China from 1982 to 2010 Based on a modified Temperature Vegetation Drought Index (mTVDI). Scientific Reports, 7(1), 17473.

Zhou, L., Wu, J.J., Mo, X.Y., Zhou, H.K., Diao, C.Y., Wang, Q.F., Chen, Y.H, Zhang, F.Y. (2017). Quantitative and detailed spatiotemporal patterns of drought in China during 2001–2013. *Science of the Total Environment, 589*, 136-145.